S-Glutathionylation of estrogen receptor α affects dendritic cell function

Received for publication, August 24, 2017, and in revised form, January 18, 2018 Published, Papers in Press, January 26, 2018, DOI 10.1074/jbc.M117.814327

Jie Zhang[‡1,2], Zhi-wei Ye[‡1], Wei Chen[§], Yefim Manevich[‡], Shikhar Mehrotra[¶], Lauren Ball[‡], Yvonne Janssen-Heininger[‖], Kenneth D. Tew[‡3], and Danyelle M. Townsend[**]

From the Departments of [‡]Cell and Molecular Pharmacology and Experimental Therapeutics, [**]Pharmaceutical and Biomedical Sciences, and [¶]Surgery, Medical University of South Carolina, Charleston, South Carolina 29425, [§]Department of Infectious Disease, the Second Affiliated Hospital of Medical School of the Southeast University, 1-1 Zhongfu Road, Nanjing 210003, China, and [‖]Department of Pathology and Laboratory Medicine, University of Vermont, Burlington, Vermont 05405

Edited by Joel Gottesfeld

Glutathione *S*-transferase Pi (GSTP) is a thiolase that catalyzes the addition of glutathione (GSH) to receptive cysteines in target proteins, producing an *S*-glutathionylated residue. Accordingly, previous studies have reported that *S*-glutathionylation is constitutively decreased in cells from mice lacking GSTP (*Gstp1/p2*$^{-/-}$). Here, we found that bone marrow–derived dendritic cells (BMDDCs) from *Gstp1/p2*$^{-/-}$ mice have proliferation rates that are greater than those in their WT counterparts (*Gstp1/p2*$^{+/+}$). Moreover, *Gstp1/p2*$^{-/-}$ BMDDCs had increased reactive oxygen species (ROS) levels and decreased GSH:glutathione disulfide (GSSG) ratios. Estrogen receptor α (ERα) is linked to myeloproliferation and differentiation, and we observed that its steady-state levels are elevated in *Gstp1/p2*$^{-/-}$ BMDDCs, indicating a link between GSTP and ERα activities. BMDDCs differentiated by granulocyte–macrophage colony-stimulating factor had elevated ERα levels, which were more pronounced in *Gstp1/p2*$^{-/-}$ than WT mice. When stimulated with lipopolysaccharide for maturation, *Gstp1/p2*$^{-/-}$ BMDDCs exhibited augmented endocytosis, maturation rate, cytokine secretion, and T-cell activation; heightened glucose uptake and glycolysis; increased Akt signaling (in the mTOR pathway); and decreased AMPK-mediated phosphorylation of proteins. Of note, GSTP formed a complex with ERα, stimulating ERα *S*-glutathionylation at cysteines 221, 245, 417, and 447; altering ERα's binding affinity for estradiol; and reducing overall binding potential (receptor density and affinity) 3-fold. Moreover, in *Gstp1/p2*$^{-/-}$ BMDDCs, ERα *S*-glutathionylation was constitutively decreased. Taken together, these findings suggest that GSTP-mediated *S*-glutathionylation of ERα controls BMDDC differentiation and affects metabolic function in dendritic cells.

Dendritic cells (DCs)[4] are antigen-presenting cells that bridge innate and adaptive immunity and can be activated by a variety of antigenic threats. Agents such as GM-CSF can facilitate enhanced differentiation of bone marrow derived–dendritic cells (BMDDCs) from hematopoietic stem cells (HSCs), and newly developed BMDDCs are often critical in mounting an effective lymphocyte-mediated immune response during infection (1, 2). The majority of mature DCs have a short half-life in peripheral blood circulation (3), and partly as a consequence regulation of BMDDC developmental pathways is a critical determinant of the total numbers of mature DCs.

There is significant documentation that drugs that influence redox conditions, and particularly thiol levels, influence bone marrow function, T-cell activation, and generally adaptive immune responses (4, 5). However, there has been no consensus as to how regulating thiol metabolism causes such adaptations. Within the marrow compartment, there exist gradient niches of calcium, oxygen, and glutathione (GSH) (6–9), each of which can influence the localization of progenitor cells and their pathways to maturity/release into the peripheral circulation. A number of redox-active drugs have been used clinically to treat various human myeloproliferative pathologies, including *N*-acetylcysteine, amifostine, and NOV-002 (10–12), each of which influences thiol homeostasis in the bone marrow compartment (8). Glutathione *S*-transferase Pi (GSTP) is a thiolase that can catalyze the addition of GSH to receptive cysteines in target proteins, producing an *S*-glutathionylated residue (13). Telintra® is a peptidomimetic inhibitor of GSTP (14) and has proven clinical activity in patients with myelodysplastic syndrome (15, 16). Conversely, mice lacking glutathione *S*-transferase Pi (*Gstp1/p2*$^{-/-}$) have a more highly prolifer-

This work was supported in part by National Institutes of Health Grants CA085660 and CA117259; National Center for Research Resources Grant P20RR024485; the Center of Biomedical Research Excellence in Oxidants, Redox Balance, and Stress Signaling, particularly the Analytical Redox Biology Core; and the South Carolina Centers of Excellence program. The authors declare that they have no conflicts of interest with the contents of this article. The content is solely the responsibility of the authors and does not necessarily represent the official views of the National Institutes of Health.

This article contains Figs. S1–S3 and Table S1.

[1] Both authors contributed equally to this work.

[2] Supported by Swedish Research Council Grant 524-2011-699.

[3] To whom correspondence should be addressed: Dept. of Cell and Molecular Pharmacology and Experimental Therapeutics, Medical University of South Carolina, 70 President St., DDB410, Charleston, SC 29425. Tel.: 843-792-2514; Fax: 843-795-2475; E-mail: tewk@musc.edu.

[4] The abbreviations used are: DC, dendritic cell; AGC, automatic gain control; BM, bone marrow; BMDDC, bone marrow–derived dendritic cell; CFSE, carboxyfluorescein diacetate succinimidyl ester; CID, collision-induced dissociation; ECAR, extracellular acidification rate; ER, estrogen receptor; ETD, electron transfer dissociation; GLUT, glucose transporter; GSTP, glutathione *S*-transferase Pi; HSC, hematopoietic stem cell; imDC, immature bone marrow–derived dendritic cell; mDC, mature bone marrow–derived dendritic cell; OCR, oxygen consumption rate; OXPHOS, oxidative phosphorylation; ROS, reactive oxygen species; TCR, T-cell receptor; UPR, unfolded protein response; MFI, mean fluorescence intensity; AMPK, AMP-activated protein kinase; APC, allophycocyanin; PE, phycoerythrin; RNS, reactive nitrogen species; DCFH, dichlorodihydrofluorescin; TG-1, ThioGlo-1; 2-NBDG, 2-(*N*-(7-nitrobenz-2-oxa-1,3-diazol-4-yl)amino)-2-deoxyglucose; NK, natural killer.

Table 1

Relative expression of genes for estrogen receptor signaling pathway in BMDDCs (Gstp1p2$^{-/-}$ *versus* Gstp1p2$^{+/+}$)

mRNAs from WT or *Gstp1/p2*$^{-/-}$ BMDDCs were extracted and quantified using the estrogen receptor signaling PCR array. Quantitative analyses of each gene were performed using Bio-Rad PrimePCR Analysis software (v.1.0.030.1023). MMTV, murine mammary tumor virus.

Gene	Symbol	Expression
Estrogen receptor 2 (β)	*Esr2*	0.135
Prostaglandin-endoperoxide synthase 2	*Ptgs2*	0.144
Trefoil factor 1	*Tff1*	0.165
WNT1-inducible signaling pathway protein 2	*Wisp2*	0.188
Adenosine A1 receptor	*Adora1*	0.254
Insulin-like growth factor–binding protein 4	*Igfbp4*	0.447
Latent transforming growth factor β–binding protein 1	*Ltbp1*	0.466
Caveolin 1, caveolae protein	*Cav1*	0.497
Heat shock protein 90, α (cytosolic), class A member 1	*Hsp90aa1*	0.499
Complement component 3	*C3*	0.517
Glucuronidase, β	*Gusb*	0.539
Nuclear receptor subfamily 0, group B, member 2	*Nr0b2*	0.543
Creatine kinase, brain	*Ckb*	0.549
Early growth response 3	*Egr3*	0.587
Nuclear receptor subfamily 5, group A, member 2	*Nr5a2*	0.613
Insulin receptor substrate 1	*Irs1*	0.646
Jun-B oncogene	*Junb*	0.674
Glucose-6-phosphate dehydrogenase X-linked	*G6pdx*	0.680
Thrombospondin 1	*Thbs1*	0.682
FBJ osteosarcoma oncogene	*Fos*	0.696
Lipoprotein lipase	*Lpl*	0.706
Cbp/p300–interacting transactivator	*Cited2*	0.725
Breast cancer antiestrogen resistance 1	*Bcar1*	0.730
Insulin-like growth factor 1	*Igf1*	0.761
Heat shock protein 90, α (cytosolic), class B member 1	*Hsp90ab1*	0.763
Cathepsin D	*Ctsd*	0.782
v-*maf* musculoaponeurotic fibrosarcoma oncogene family	*Maff*	0.795
PrimePCR RNA Quality Assay	RQ1	0.805
Secreted phosphoprotein 1	*Spp1*	0.816
Cytochrome P450, family 1, subfamily a, polypeptide 1	*Cyp1a1*	0.816
β_2-Microglobulin	*B2m*	0.816
Connective tissue growth factor	*Ctgf*	0.825
Follistatin	*Fst*	0.825
L1 cell adhesion molecule	*L1cam*	0.828
Kallikrein B, plasma 1	*Klkb1*	0.854
Actin, β	*Actb*	0.866
BCL2-like 1	*Bcl2l1*	0.878
Vitamin D receptor	*Vdr*	0.883
Cyclin D1	*Ccnd1*	0.884
Lectin, galactose-binding, soluble 1	*Lgals1*	0.905
Breast cancer 1	*Brca1*	0.922
S100 calcium-binding protein A6 (calcyclin)	*S100a6*	0.922
Forkhead box A1	*Foxa1*	0.940
Myelocytomatosis oncogene	*Myc*	0.971
Estrogen receptor–binding fragment-associated gene 9	*Ebag9*	0.975
Nuclear receptor corepressor 2	*Ncor2*	1.009
Nuclear receptor coactivator 3	*Ncoa3*	1.021
Vascular endothelial growth factor A	*Vegfa*	1.031
Aryl-hydrocarbon receptor	*Ahr*	1.068
Metastasis-associated 1	*Mta1*	1.173
X-box–binding protein 1	*Xbp1*	1.177
Suppressor of cytokine signaling 3	*Socs3*	1.190
Scaffold attachment factor B	*Safb*	1.203
Bone morphogenetic protein 4	*Bmp4*	1.205
PDZ domain–containing 1	*Pdzk1*	1.214
Chemokine (CC motif) ligand 12	*Ccl12*	1.227
Patched homolog 1	*Ptch1*	1.227
Wingless-related MMTV integration site 5A	*Wnt5a*	1.266
Bone morphogenetic protein 7	*Bmp7*	1.291
PrimePCR Reverse Transcription Control Assay	RT	1.335
Wingless-related MMTV integration site 4	*Wnt4*	1.335
Transforming growth factor, β3	*Tgfb3*	1.345
v-*erb-b2* erythroblastic leukemia viral oncogene homolog 2	*Erbb2*	1.372
Nuclear receptor coactivator 1	*Ncoa1*	1.391
Nuclear receptor subfamily 3, group C, member 1	*Nr3c1*	1.402
Proline-, glutamic acid-, and leucine-rich protein 1	*Pelp1*	1.403
Nuclear receptor–interacting protein 1	*Nrip1*	1.446
Nuclear receptor coactivator 2	*Ncoa2*	1.449
Neuropilin 1	*Nrp1*	1.460
Hypoxanthine-guanine phosphoribosyltransferase	*Hprt*	1.465
Mediator complex subunit 1	*Med1*	1.591
Transforming growth factor, α	*Tgfa*	1.591
v-*ral* simian leukemia viral oncogene homolog A	*Rala*	1.615
PrimePCR Positive Control Assay	PCR	1.622
Ngfi-A–binding protein 2	*Nab2*	1.628
A kinase (PRKA) anchor protein 1	*Akap1*	1.690
Progesterone receptor	*Pgr*	1.696
Amyloid β (A4) precursor protein–binding, family B1	*Apbb1*	1.812
Insulin-like growth factor–binding protein 5	*Igfbp5*	1.955
Prohibitin 2	*Phb2*	2.082
Matrix metallopeptidase 9	*Mmp9*	2.168
PrimePCR RNA Quality Assay	RQ2	2.170
Brain-derived neurotrophic factor	*Bdnf*	2.255
Nuclear receptor subfamily 2, group F, member 6	*Nr2f6*	2.297
Ephrin A5	*Efna5*	2.598
Nephroblastoma overexpressed gene	*Nov*	2.717
Retinoic acid receptor, α	*Rara*	3.243
Snail homolog 1 (*Drosophila*)	*Snai1*	4.669
Estrogen receptor 1 (α)	*Esr1*	5.416
v-*erb-b2* erythroblastic leukemia viral oncogene homolog 3	*Erbb3*	12.099

ative bone marrow, resulting in higher levels of circulating blood cells of all lineages (14, 17). These findings collectively suggest that GSTP-controlled protein *S*-glutathionylation regulates bone marrow progenitor cell function.

Hematopoietic progenitor cells also express estrogen receptor α (ERα), and ERα signaling is known to influence both development and maturation of BMDDCs and the general sustainability of an immune response (18). ERα broadly impacts glucose metabolism and metabolic gene expression patterns that stimulate resting T cells toward rapid proliferation and differentiation into mature T-effector populations (19). Although a number of studies suggest that downstream transcriptional events triggered by higher levels of ERα and estrogens contribute to enhanced proliferation and functions of BMDDCs, it remains unclear how redox conditions and hormone-based pathways might bisect.

The goal of the present study was to elucidate whether GSTP regulates ERα and whether this in turn regulates proliferation, differentiation, and effector function of BMDDCs. We demonstrate that GSTP and ERα interact and that GSTP induces *S*-glutathionylation of critical cysteines within ERα. *S*-Glutathionylation of ERα decreases affinity of ERα for estradiol. We furthermore demonstrate that the absence of GSTP enhanced energy metabolism (glucose use and transition to glycolysis) and proliferative and differentiation rates and increased DC effector function in association with decreased ERα-SSG.

Results

A principle rationale for the initiation of the present studies was that analysis of an estrogen receptor signaling primer array comparing wildtype and knockout BMDDCs (Table 1 and Fig. S1) quantitatively demonstrated the existence of a nexus between GSTP and ERα: the most affected change caused by ablation of GSTP was increased expression of ERα, and this was

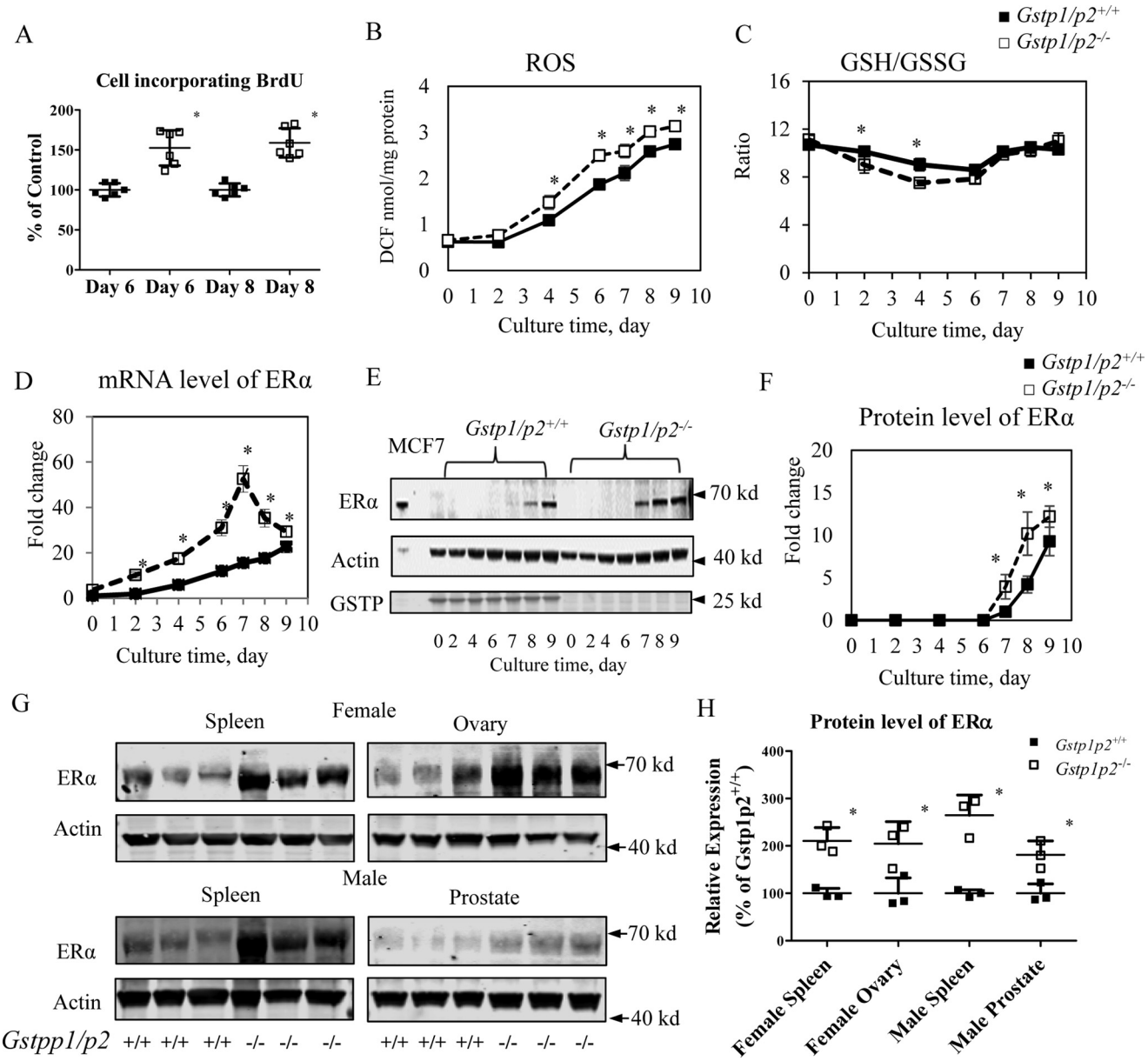

Figure 1. ERα levels and oxidative stress are higher in *Gstp1/p2*$^{-/-}$ cells during GM-CSF–driven BMDDC differentiation and proliferation. BM cells were prepared from femora and tibiae from *Gstp1/p2*$^{-/-}$ or WT mice and cultured in the presence of GM-CSF as described under "Experimental procedures." Non-adherent cells were collected at days 0, 2, 4, 6, 7, 8, and 9, respectively. *A*, *Gstp1/p2*$^{-/-}$ BMDDCs differentiated with GM-CSF had higher proliferation rates. On days 4 and 6, BM cells were seeded at 0.2×10^6 cells/ml in DC medium and cultured for an extra 2 days. Cell proliferation was then assessed by BrdU incorporation. *B*, cellular ROS levels were measured using a proprietary quenched fluorogenic probe, DCFH-DiOxyQ. *C*, intracellular GSH levels were measured by thiol fluorescent probe IV after protein precipitation. Intracellular GSSG levels were determined based on the reduction of GSSG in the presence of glutathione reductase and NADPH. Data are presented as GSH/GSSG ratio. *D*, ERα mRNA levels were determined by quantitative RT-PCR. *E* and *F*, ERα protein levels were evaluated by immunoblotting and quantified with Image Studio 4.0 software. The breast cancer cell line MCF7 was used as a positive control for ERα. *G* and *H*, *Gstp1/p2*$^{-/-}$ mice have higher resting tissue levels of ERα. Tissue samples (spleen, ovary, or prostate) were freshly prepared from *Gstp1/p2*$^{-/-}$ or WT mice. ERα protein levels were evaluated by immunoblotting and quantified with Image Studio 4.0 software. Actin served as a loading control. Data shown are means ± S.D. from three animals. *Error bars* represent S.D. *, significant differences between *Gstp1/p2*$^{-/-}$ and WT, $p < 0.05$. *DCF*, dichlorofluorescein.

accompanied by a decrease in expression of ERβ. A number of transcription and growth factors and accessory proteins were also increased (Table 1), including tyrosine kinase receptors of the ERB family and PELP1, a coactivator of ERα. Such data encouraged us to interrogate those factors that provided a link between GSTP-mediated redox regulation and estrogen receptor function, particularly as existing evidence already implicates each in bone marrow proliferation.

Gstp1/p2-null mice have higher levels of oxidative stress and ERα during BMDDC differentiation

Bone marrow (BM) cells from GSTP-null mice proliferate faster (shorter doubling times) and produce more circulating blood cells of all lineages than the WT (17). Fig. 1*A* shows that enhanced proliferation rates in *Gstp1/p2*$^{-/-}$ cells were maintained when BMDDCs were differentiated from BM precursors in the presence of GM-CSF with incorporation of BrdU used as

a marker. Differentiation of DCs is essentially complete at day 6 but can continue until day 9. In our present study, we focused on immature bone marrow–derived dendritic cells (imDCs), therefore we selected cells from days 6 and 8, each representing typical growth of imDCs. During the differentiation of BMDDCs from precursor cells, GM-CSF treatment caused a time-dependent increase in ROS in both GSTP WT and KO cells, and the change was more pronounced in cells from *Gstp1/p2*$^{-/-}$ mice (Fig. 1*B*). There was also a shift in the GSH/GSSG ratios toward a more oxidized state (Fig. 1*C*). We consistently observed that ROS levels were higher in the GSTP KO BMDDCs. It seems that GSH/GSSG ratios drop at the early days (mainly during HSC to DC differentiation from days 0 to 6) and then increase and stabilize during DC cell proliferation (days 6–9). However, the ROS levels consistently increased during the entire period of GM-CSF–induced differentiation and proliferation. In general, the data suggested that GM-CSF induced oxidative stress, causing a disruption in redox balance that was more pronounced in GSTP-deficient cells. In concordance with the comparative array data (Table 1), GM-CSF–induced differentiation of BMDDCs from BM precursors caused a gradual increase in expression of ERα, both at the transcript (Fig. 1*D*) and protein levels (Fig. 1, *E* and *F*). The up-regulation of mRNA is much greater in GSTP KO mice, and the highest levels occur on day 7. However, there is a lag of protein expression *versus* gene up-regulation, most pronounced after day 7. At early time points, low ERα expression and limited detection capacities of the ERα antibodies meant that we could not detect a band. ERα levels were higher in the *Gstp1/p2*$^{-/-}$ cells and increased at a faster rate in the time after GM-CSF stimulation. *Gstp1/p2*$^{-/-}$ cells had detectable protein levels from day 7 onward, whereas *Gstp1/p2*$^{+/+}$ cells had detectable protein levels only from day 8 (Fig. 1, *E* and *F*). This seemed to be a characteristic of the *Gstp1/p2*$^{-/-}$ mice because higher resting-state levels of ERα were found in spleen, ovary, and prostate (Fig. 1, *G* and *H*).

Gstp1/p2 depletion in BMDDCs results in a proinflammatory phenotype

ERα has been suggested previously to play a role in regulating DC endocytosis, maturation, and cytokine secretion and priming T-cell proliferation (18, 19). We performed a series of experiments to measure comparative differences in BMDDC functions between WT and *Gstp1/p2*$^{-/-}$ mice. The data indicated that higher levels of DC functions occurred in the absence of GSTP expression. As a function specific to imDCs, we measured the capacity to endocytose FITC-dextran via the mannose receptor. Fig. 2, *A* and *B*, show that endocytotic functions were higher in *Gstp1/p2*$^{-/-}$ BMDDCs compared with WT. In response to an agonist of toll-like receptor 4, *Gstp1/p2*$^{-/-}$ BMDDCs matured normally following LPS treatment as demonstrated by their expression of CD80, MHCII, and CD86 (Fig. 2*C*). However, expression of these maturation markers was enhanced in LPS-treated *Gstp1/p2*$^{-/-}$ compared with WT BMDDCs (quantification (arbitrary units) of the MFI values for *Gstp1/p2*$^{-/-}$ *versus* WT: CD80, 8884 ± 308 *versus* 5068 ± 579; MHCII, 70,097 ± 891 *versus* 55,127 ± 2703; CD86, 39,359 ± 4872 *versus* 24,085 ± 4552; Fig. 2*D*). Even in the absence of LPS, *Gstp1/p2*$^{-/-}$ BMDDCs had higher levels of MHCII (Fig. 2*D*). Furthermore, following LPS activation, *Gstp1/p2*$^{-/-}$ BMDDCs produced significantly higher levels of the proinflammatory cytokine IL-12p70 and less of the anti-inflammatory cytokine IL-10 compared with their WT counterparts (*Gstp1/p2*$^{-/-}$ *versus* WT: IL-12p70, 371 ± 26 *versus* 232 ± 13; IL-10, 369 ± 22 *versus* 577 ± 53). Without LPS activation, IL-12p70 secretion was very low, and IL-10 secretion was undetectable in both WT and *Gstp1/p2*$^{-/-}$ BMDDCs (Fig. 2*E*). Finally, we investigated the efficiency with which BMDDCs primed naïve T cells by stimulating carboxyfluorescein diacetate succinimidyl ester (CFSE)–labeled naïve T cells (from *Pmel-1* T-cell receptor (TCR) transgenic mice) with hgp100(25–33)-pulsed BMDDCs activated with LPS (mature bone marrow–derived dendritic cells (mDCs)). Fig. 2*F* shows that naïve CD8$^+$ T cells undergo antigen-specific proliferation when cocultured with either WT or *Gstp1/p2*$^{-/-}$ mDCs, and higher levels of T-cell expansion were observed when cocultured with *Gstp1/p2*$^{-/-}$ mDCs. Together, these data show that *Gstp1/p2* ablation resulted in a phenotype of enhanced DC endocytosis, maturation, proinflammatory cytokine secretion, and capacity to prime T-cell proliferation.

Gstp1/p2 depletion in BMDDCs results in increased glycolysis

It seemed reasonable to expect that enhanced proliferation rates and DC activation by LPS should be accompanied by changes in cellular metabolism and bioenergetics. To support increased demands for synthesis and transport of proteins required for BMDDC maturation, recent evidence suggests that LPS activation of DCs drives a decline in oxidative phosphorylation (OXPHOS) and commitment to glycolysis (provides ATP as well as generates lipids for membrane synthesis, including endoplasmic reticulum and Golgi (20–22)). Because ERα has been shown to affect glucose metabolism (19), we reasoned that *Gstp1/p2*$^{-/-}$ BMDDCs should be metabolically different from WT. To obtain insight into functional differences between WT and *Gstp1/p2*$^{-/-}$ BMDDC mitochondria, we first mapped mitochondrial function by using a Seahorse Metabolic Analyzer to measure oxygen consumption rate (OCR), an indicator of oxidative phosphorylation, and extracellular acidification rate (ECAR), an indicator of glycolysis. For both WT and *Gstp1/p2*$^{-/-}$ BMDDCs, stimulation with LPS resulted in decreased OCR and an accompanying increased ECAR as compared with control (Fig. 3*A*). This indicated attenuated rates of OXPHOS and enhanced glycolysis. In addition, following LPS activation, *Gstp1/p2*$^{-/-}$ BMDDCs had significantly higher ECAR values when compared with WT cells, indicating their higher glycolytic capacity (Fig. 3*A*). Meanwhile, OCR values were significantly lower in *Gstp1/p2*$^{-/-}$ BMDDCs compared with WT cells (Fig. 3*A*). Furthermore, Fig. 3*B* shows the time-dependent uptake of glucose in BMDDCs. Stimulation with LPS resulted in increased glucose uptake in both WT and *Gstp1/p2*$^{-/-}$ mDCs. A comparison of glucose uptake rates revealed that *Gstp1/p2*$^{-/-}$ mDCs were more glycolytic than WT cells. For additional clarification, we used quantitative RT-PCR to measure mRNA expression levels of various glycolysis-

associated genes, including *Aldoa*, *Aldoc*, *Eno1*, *Eno3*, *Gck*, *Gpi*, *Hk2*, *Ldha*, *Ldhb*, *Ldhc*, *Pfk*, *Pgam1*, *Pgk1*, *pkm*, *Slc2a1*, and *Slc2a4*. Among these, our data showed that the mRNA expression levels of several glycolytic genes were severalfold higher in *Gstp1/p2*$^{-/-}$ BMDDCs (Fig. 3*C*), including enolase (*Eno3*), phosphoglycerate isomerase (*Pgam1*), and glucose transporter 1 (*Slc2a1*). In addition, the more pronounced up-regulation of protein levels of phosphoglycerate isomerase (PGAM1) and glucose transporter 1 (GLUT1) was confirmed in *Gstp1/p2*$^{-/-}$ BMDDCs. Due to the availability and sensitivity of antibodies, β-enolase was not detected in this study (Fig. 3, *D* and *E*).

Increased glycolysis in *Gstp1/p2*$^{-/-}$ BMDDCs was accompanied by an increased activation of the mTOR pathway. This was assessed by phosphorylation of Akt and decreased activation of AMPK as determined by phosphorylation of

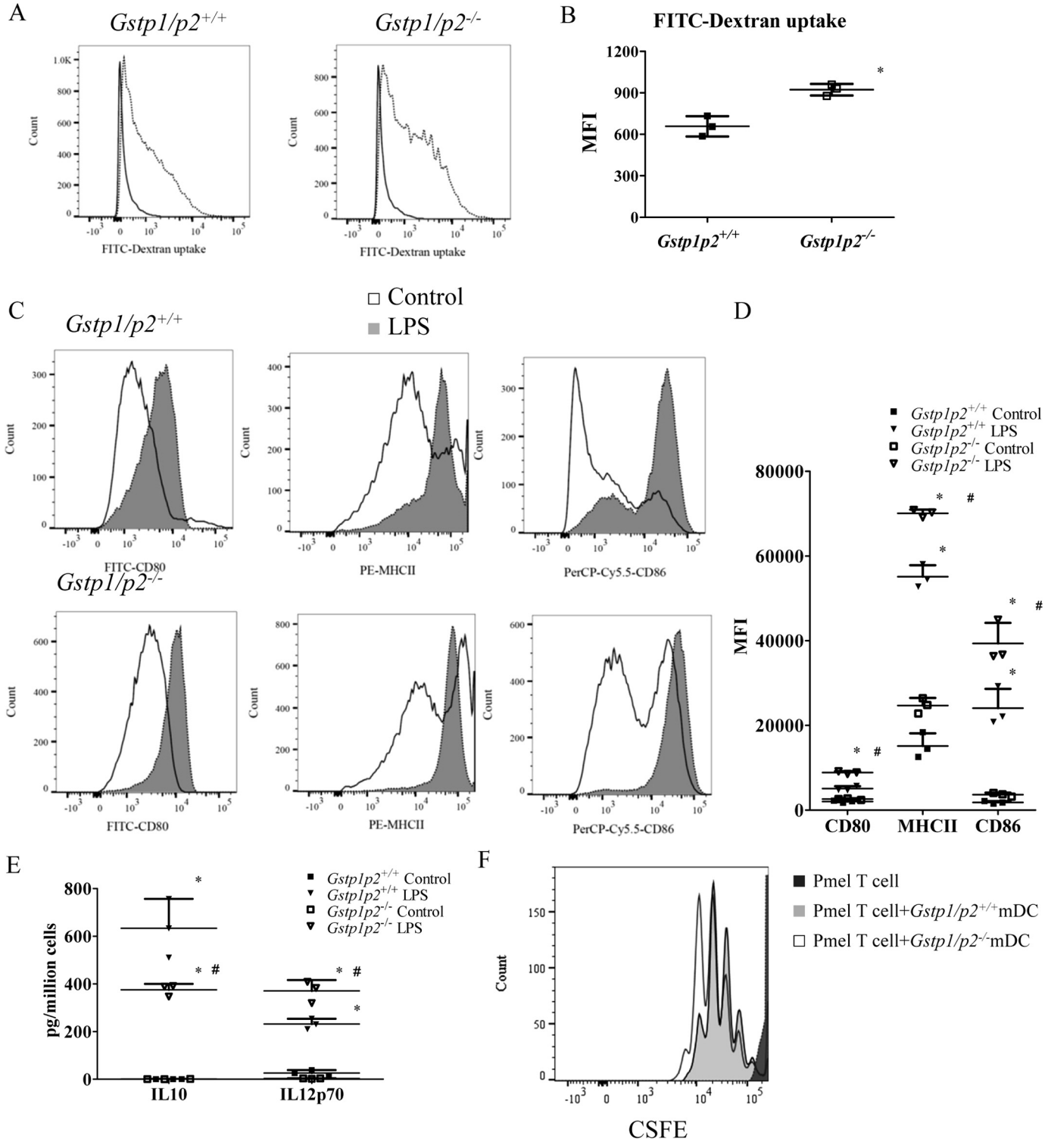

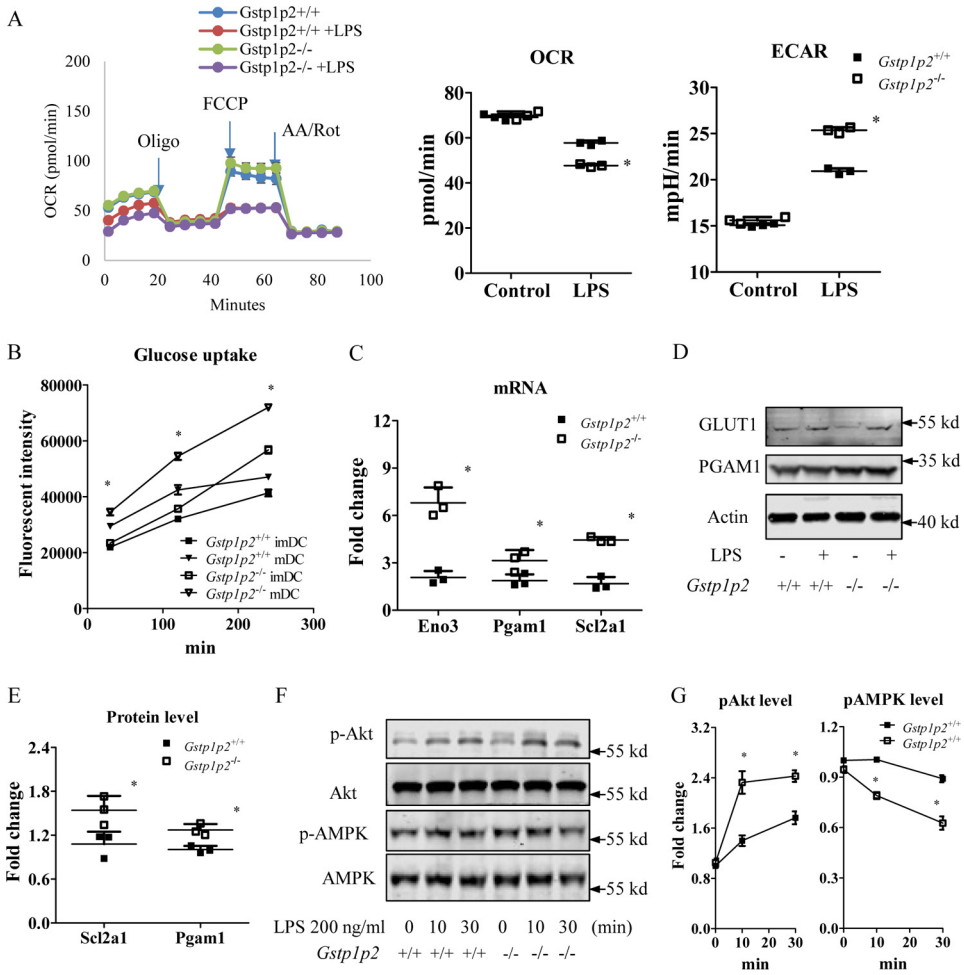

Figure 3. *Gstp1/p2*$^{-/-}$ BMDDCs are more glycolytic after LPS activation. *A*, BMDDCs were seeded in a Seahorse XF96 microplate and stimulated overnight with DC medium (as a control) or 200 ng/ml LPS, and real-time OCR during sequential treatments with oligomycin (*Oligo*; ATP synthase inhibitor), carbonyl cyanide *p*-trifluoromethoxyphenylhydrazone (*FCCP*), and antimycin A/rotenone (*AA/Rot*; electron transport chain inhibitors) and basal OCR and ECAR were determined by the Seahorse XF96 analyzer. Data shown are means ± S.D. of three experiments. *Error bars* represent S.D. *, significant differences between *Gstp1/p2*$^{-/-}$ and WT mDCs, $p < 0.05$. *mpH*, milliunit of pH value. *B*, glucose uptake levels were evaluated using the fluorescently labeled deoxyglucose analog 2-NBDG. Data shown are means ± S.D. of three experiments. *Error bars* represent S.D. *, significant differences between *Gstp1/p2*$^{-/-}$ and WT mDCs, $p < 0.05$. *C*, quantitative RT-PCR analysis of the expression of key genes associated with glycolysis. Data shown are means ± S.D. of three experiments. *Error bars* represent S.D. *, significant differences between *Gstp1/p2*$^{-/-}$ and WT mDCs, $p < 0.05$. *D* and *E*, the protein levels of associated genes were further evaluated by immunoblotting with GLUT1, PGAM1, and β-enolase antibodies and quantified with Image Studio 4.0 software. β-Enolase was not detectable in BMDDCs. Results are representative of three experiments. *, significant differences between *Gstp1/p2*$^{-/-}$ and WT mDCs, $p < 0.05$. *F* and *G*, phosphorylation (*p*) levels of Akt and AMPK were evaluated by immunoblotting and quantified with Image Studio 4.0 software. Data shown are means ± S.D. of three experiments. *Error bars* represent S.D. *, significant differences between *Gstp1/p2*$^{-/-}$ and WT DCs, $p < 0.05$.

AMPK (Fig. 3, *F* and *G*). Akt activation promotes the shift to glycolysis and anabolic metabolism required for DC activation and immunogenicity, whereas AMPK activation antagonizes these responses (21). These results support the concept that ablation of GSTP contributes directly to the shift toward these pathways.

Figure 2. BMDDCs from *Gstp1/p2*$^{-/-}$ mice have enhanced antigen presentation functions. *A*, endocytosis was evaluated by FITC-dextran uptake. BMDDCs from *Gstp1/p2*$^{-/-}$ or WT mice were pulsed with 1 mg/ml FITC-dextran for 4 h at either 37 or 4 °C and counterstained for markers for DCs (CD11c), T cells (CD3e), B cells (CD45R/B220), monocytes/macrophages (CD14), and NK cells (NK1.1 molecules) before analysis by flow cytometry. Plots are gated on CD11c$^+$, CD3e$^-$, CD45R/B220$^-$, CD14$^-$, and NK1.1$^-$ cells. Representative histograms of three experiments are shown. *B*, FITC-dextran uptake at 37 °C compared with 4 °C (control) shows the mean MFI ± S.D. from three experiments. *Error bars* represent S.D. *, significant differences between *Gstp1/p2*$^{-/-}$ and WT imDCs, $p < 0.05$. *C*, BMDDCs were cultured in DC medium with or without 200 ng/ml LPS overnight and then analyzed for the expression of maturation markers by flow cytometry. Plots are gated on CD11c$^+$ cells. Data are representative of three experiments. *D*, quantitative graphical representation of *C*. Data shown are mean MFI ± S.D. from three experiments. *Error bars* represent S.D. *, significant differences between control and LPS treatment, $p < 0.05$; #, significant differences between *Gstp1/p2*$^{-/-}$ and WT DCs after LPS treatment, $p < 0.05$. *E*, BMDDCs from *Gstp1/p2*$^{-/-}$ or WT mice were stimulated with 200 ng/ml LPS overnight, and medium was removed and examined by ELISA for the proinflammatory cytokine IL-12p70 and the anti-inflammatory cytokine IL-10. Data shown are means ± S.D. of three experiments. *Error bars* represent S.D. *, significant differences between control and LPS treatment, $p < 0.05$; #, significant differences between *Gstp1/p2*$^{-/-}$ and WT DCs after LPS treatment, $p < 0.05$. *F*, BMDDCs treated with 200 ng/ml LPS overnight were pulsed with 1 μg/ml hgp100(25–33) peptide in T-cell medium for 2 h and then cocultured with CFSE-labeled, hgp100(25–33)-specific *Pmel-1* TCR transgenic T cells (DC/T cell ratio = 1:5) for 3 days. T-cell proliferation by CFSE dilution was measured by flow cytometry. Plots are gated on CD8$^+$ cells. The proliferation profiles shown are representative of three experiments.

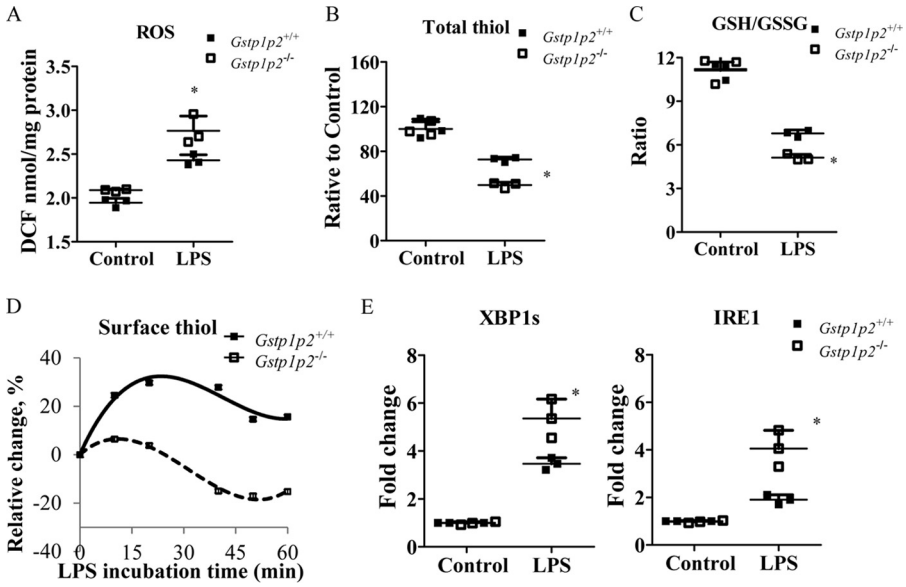

Figure 4. BMDDCs from *Gstp1/p2*$^{-/-}$ mice have higher levels of oxidative stress and UPR during LPS activation. *A*, cellular ROS levels were measured using a proprietary quenched fluorogenic probe, DCFH-DiOxyQ. *B*, intracellular reduced thiol levels were measured by thiol fluorescent probe IV. *C*, intracellular GSH levels were measured by thiol fluorescent probe IV after protein precipitation. Intracellular GSSG levels were determined based on the reduction of GSSG in the presence of glutathione reductase and NADPH. Data are presented as GSH/GSSG ratio. *D*, total surface reduced thiol levels were determined by an immediate fluorescence increase upon addition of ThioGlo-1. *E*, UPR genes IRE1 and XPB1s were quantified by quantitative RT-PCR. Data shown are means ± S.D. of three experiments. *Error bars* represent S.D. *, significant differences between *Gstp1/p2*$^{-/-}$ and WT after LPS treatment, $p < 0.05$. *DCF*, dichlorofluorescein.

Gstp1/p2$^{-/-}$ *BMDDCs show different redox responses after LPS stimulation*

Compared with WT, *Gstp1/p2*$^{-/-}$ BMDDCs had higher endogenous levels of ROS (Fig. 4*A*) even before LPS treatment. When stimulated with LPS, there was a further increase in ROS coincident with a decrease in both total cellular thiols (Fig. 4*B*) and cell surface thiols (Fig. 4*D*), and the GSH/GSSG ratio was shifted toward a more oxidized state (Fig. 4*C*). Thus, LPS caused a general shift in oxidative conditions, but each measure was more pronounced in the *Gstp1/p2*$^{-/-}$ cells. Furthermore, LPS also induced an unfolded protein response (UPR) in BMDDCs. This is exemplified by the IRE1/XBP1 pathway response where *Gstp1/p2*$^{-/-}$ BMDDCs exhibited a more marked activation compared with WT (Fig. 4*E*). These results were similar to our earlier studies (24) where both thapsigargin and tunicamycin caused a more pronounced UPR in *GSTp1/p2*$^{-/-}$ BMDDCs compared with wildtype. IRE1/XBP1 activation has been shown to be essential for the development of DCs and regulation of innate immune responses in macrophages (39, 42). Therefore, the higher UPR activation with LPS in *Gstp1/p2*$^{-/-}$ cells might be correlated to its enhanced functionality as well.

ERα is subject to S-glutathionylation under oxidative stress

Fig. 5*A* shows that, in WT BMDDCs, GSTP and ERα coimmunoprecipitated with antibodies to ERα, indicating that they form part of a protein complex. Presumably as a consequence of this interaction, further immunoprecipitation with anti-GSH antibodies showed that, following ROS generation by disulfiram, ERα was a substrate for *S*-glutathionylation (Fig. 5, *B* and *C*). In the *Gstp1/p2*$^{-/-}$ cells, there was no complex formation (Fig. 5*A*), and levels of ERα *S*-glutathionylation were significantly lower (Fig. 5, *B* and *C*).

Proteomic identification of cysteine S-glutathionylation in ERα

Of the 595 amino acids in human ERα, there are 13 cysteines, all of which are conserved between mouse and human. Human recombinant ERα proteins were treated with disulfiram and separated on a non-reducing gel, and *S*-glutathionylation of ERα was confirmed by Western blotting using anti-GSH antibodies (Fig. 5*D*, *left panel*). The gel was stained with colloidal Coomassie stain, and the result confirmed even loading of ERα under both control and disulfiram-treated conditions (Fig. 5*D*, *right panel*). Protein bands (as indicated in the *box*) were excised, destained, enzymatically digested, and subjected to LC-MS/MS identification. Mass spectrometric analysis of recombinant ERα revealed that cysteines 185, 188, 202, 205, 221, 227, 237, and 240 were involved in intra- or intermolecular disulfide linkages. Following fragmentation, these cysteines were observed with either a sulfide or had lost the thiol group. Cys-381 was not detected, and Cys-530 was oxidized. Cysteines 221, 245, 417, and 447 were *S*-glutathionylated and yielded a diagnostic glutathione ion at m/z 308 following electron transfer dissociation (Fig. 5*E* and Table 2). Characteristic fragmentation patterns of *S*-glutathionylated peptides, details of the observed sites of cysteine modification, and tandem mass spectra are provided in Figs. S2 and S3.

Cysteine S-glutathionylation causes functional changes in ERα

To determine whether this post-translational modification caused functional changes in ERα function, we performed estrogen binding assays. Fig. 5*F* shows the radioligand binding results, establishing that *S*-glutathionylation reduced the total density of receptors (B_{max}, 1805 *versus* 1532) and altered the equilibrium dissociation constant (K_d,

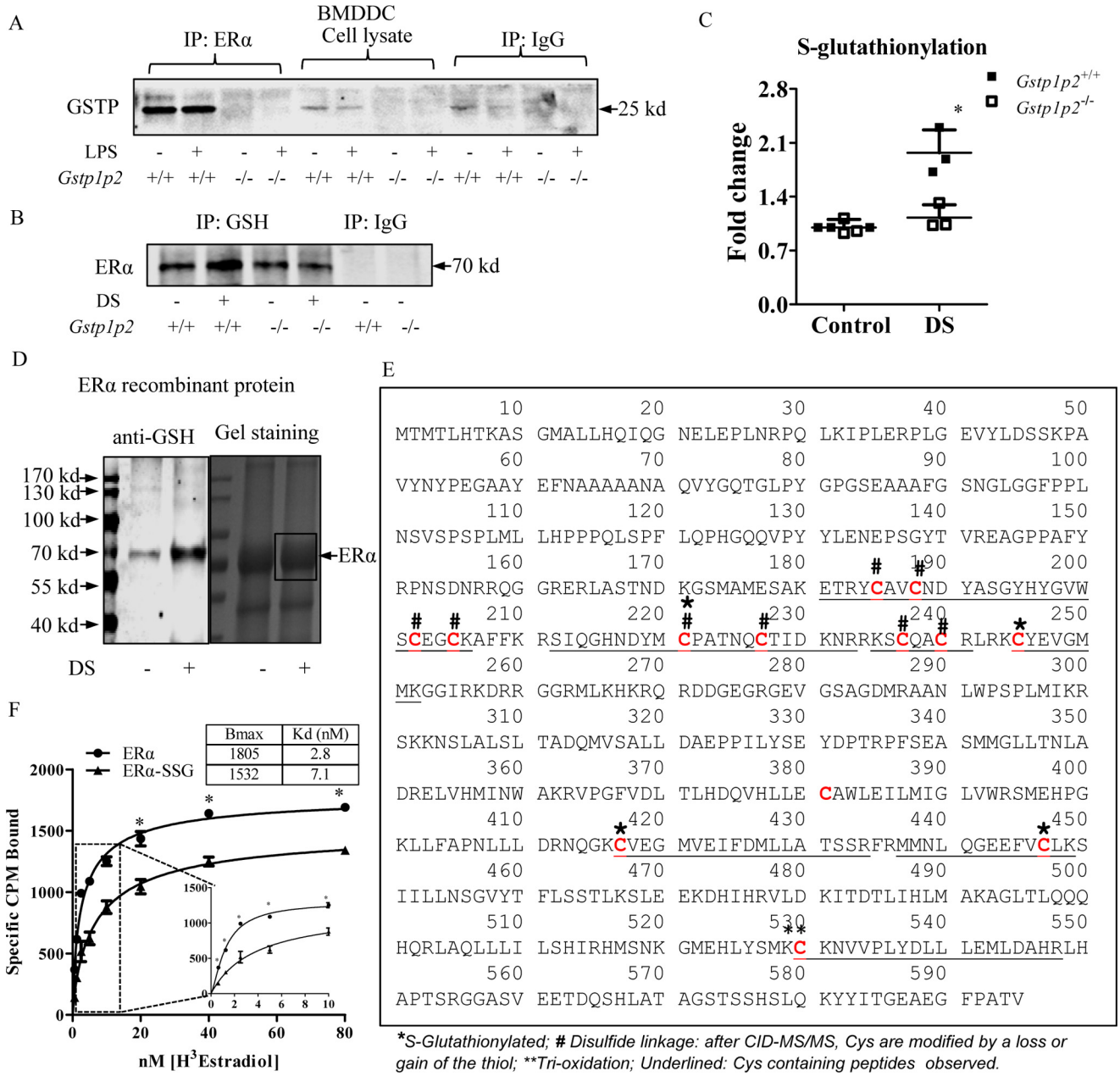

Figure 5. GSTP catalyzes ERα *S*-glutathionylation through protein-protein interaction and regulates ERα binding affinity for estradiol. *A*, 500 μg of BMDDC lysates, untreated or treated with 200 ng/ml LPS (overnight), from WT and *Gstp1/p2*$^{-/-}$ mice were used for immunoprecipitation (*IP*) with anti-ERα antibodies. Samples were analyzed by SDS-PAGE with the IgG controls and blotted for GSTP. *B* and *C*, 500 μg of BMDDC lysates, untreated or treated with disulfiram (*DS*) to promote *S*-glutathionylation (10 μM for 30 min at 37 °C), from WT and *Gstp1/p2*$^{-/-}$ mice were used for immunoprecipitation with anti-GSH antibodies. Samples were analyzed by SDS-PAGE with the IgG controls, blotted for ERα, and quantified with Image Studio 4.0 software. Results are representative of three experiments. *, significant differences between *Gstp1/p2*$^{-/-}$ and WT, $p < 0.05$. *D*, recombinant ERα proteins, untreated and *S*-glutathionylated (10 μM disulfiram and 10 mM GSH for 30 min at 37 °C), were separated on a non-reducing gel. One part of the gel was transferred to a PVDF membrane and blotted with anti-GSH antibody (*left panel*), and the other part of the gel was stained by colloidal Coomassie stain (*right panel*). Bands (as indicated in the *box*) were excised, destained, enzymatically digested, and subjected to LC-MS/MS identification. *E*, proteomic identification of sites of cysteine modification on ERα (*, *S*-glutathionylated; #, disulfide linkage; **, trioxidation). *F*, saturation binding assays of estradiol. Recombinant ERα protein (untreated or *S*-glutathionylated) was incubated with [^{3}H]estradiol (from 0.625 to 80 nM) at room temperature for 90 min, and bound estradiol was measured by liquid scintillation counting. Data were analyzed using a specific binding module from Prism 5.0. Maximum amounts of estradiol bound receptor (B_{max}) and binding affinities (K_d) were calculated. Data shown are means ± S.D. of three experiments. *Error bars* represent S.D. *, significant differences between ERα and ERα-SSG, $p < 0.05$.

2.8 *versus* 7.1 nM). From these results, we calculated that *S*-glutathionylation of ERα reduced the overall binding potential for estrogen (receptor density × affinity) 3-fold, from 645 to 216. Overall, these findings suggest that GSTP-mediated *S*-glutathionylation of ERα decreases ERα activity.

Discussion

A primary rationale for the present study was derived from the original observation that genetic ablation of GSTP caused increased expression of ERα and implied the existence of a significant link between the two. In this context, mice deficient in

Table 2
Cysteine modifications observed in human ERα (P03372)
Tandem mass spectra are provided in the supporting information. Dha, dehydroalanine.

Residues	Cys positions	Site of S–GSH	All modifications	Peptide sequence	MS/MS	Precursor *m*/*z* (MS/MS)	*z*	Enzyme
184–206	185, 188, 202, 205		Sulfide (Cys); Cys to Dha (Cys)	YCAVCNDYASGYHYGVWSCEGCK	CID	1288.48	2	Trypsin
190–206	202, 205		Sulfide (Cys); Cys to Dha (Cys)	DYASGYHYGVWSCEGCK	ETD	641.59	3	Lys-C, Asp-N
212–231	221, 227		Sulfide (Cys); Cys to Dha (Cys); trioxidation (Cys)	SIQGHNDYMCPATNQCTIDK	CID	1127.47	2	Trypsin
212–233	221, 227	221	*S*-Glutathione (Cys); Cys to Dha (Cys)	SIQGHNDYMCPATNQCTIDKNR	ETD	696.05	3	Trypsin
235–241	237, 240		Sulfide (Cys); Cys to Dha (Cys)	KSCQACR	CID	397.17	2	Trypsin
245–252	245	245	*S*-Glutathione (Cys)	CYEVGMMK	ETD	422.49	2	Trypsin
245–252	245	245	*S*-Glutathione (Cys); oxidation (Met)	CYEVGMMK	ETD	427.82	2	Trypsin
417–434	417	417	*S*-Glutathione (Cys)	CVEGMVEIFDMLLATSSR	CID	1154.01	2	Trypsin
417–434	417	417	*S*-Glutathione (Cys); oxidation (Met)	CVEGMVEIFDMLLATSSR	ETD	769.68	3	Trypsin
437–449	447	447	*S*-Glutathione	MMNLQGEEFVCLK	CID	923.89	2	Trypsin
437–449	447	447	*S*-Glutathione (Cys); oxidation (Met)	MMNLQGEEFVCLK	ETD	621.6	3	Trypsin
530–548	530		Trioxidation (Cys); oxidation (Met)	CKNVVPLYDLLLEMLDAHR	CID	770.06	3	Lys-C, trypsin

either GSTP or ERα are known to be more susceptible to infections, suggesting that innate immunity is impaired (25, 26). Moreover, ERα signaling controls the development of dendritic cells, initiating the processes of innate and adaptive immunity (18), and regulates the expression of genes that influence lymphocyte metabolism and activation (27). In both human and mouse bone marrow, HSCs express ERα with levels coincident with the processes that lead to development of a mature immune system in neonatal life (28, 29). Greater levels of ERα signaling can regulate HSC numbers and BMDDC development and result in greater numbers of dendritic cells that will modulate the scale and/or quality of either adaptive or innate immunity (29). Our present results suggest linkages for these diverse observations and illustrate how altered redox homeostasis influences ERα and the processes that lead to BMDDC differentiation.

Although we found that resting levels of ERα were elevated in all tissues of the *Gstp1*/*p2*$^{-/-}$ mouse, our results also showed that GSTP-deficient mice were more sensitive to the effects of LPS at amplifying pathways leading to BMDDC activation. Although GSTP has some detoxification enzyme properties, LPS is not a substrate. Instead, its capacity to act as a thiolase and catalyze *S*-glutathionylation of ERα can provide an explanation for the observed effects. We showed that GSTP forms a complex with ERα, but in perspective, ERα interacts with ~700 proteins, so in and of itself, its interaction with GSTP may not be remarkable. In the same vein, GSTP also has a tendency to form protein complexes with a large number of proteins, primarily because such proteins tend to be substrates for *S*-glutathionylation. In this regard, the donation of the –SG moiety to an activated cysteine thiolate anion would imply that part of ERα is recognized by the designated H-site on GSTP. This catalysis is facilitated by GSTP forming a temporal, reversible association with ERα, allowing for the transfer of the –SG moiety from the enzyme's "G" site (30). Whether GSTP and ERα form a direct or indirect (part of a larger protein cluster) complex (24, 31), it is apparent that the latter is a substrate for *S*-glutathionylation. Because *S*-glutathionylation has a profound impact on the structure, function, and subcellular distribution of most proteins (13, 32), it seems reasonable to suggest that ERα will be similarly impacted. Of the 595 amino acids in human ERα, there are 13 cysteines, all of which are conserved between mouse and human. In this study, we identified four cysteines that were susceptible to *S*-glutathionylation, residues 221, 245, 417, and 447. Cysteine 530 of the human ERα is the main covalent attachment site of photoaffinity-labeled estradiol and is in close proximity to Cys-417 and Cys-447, each located at the border (or in structural elements) delineating the hormone-binding pocket (33). *S*-Glutathionylation of any of these residues would also serve to impact the conformation of the binding pocket, influencing steroid recognition and binding as well as subcellular localization. Cysteines 221 and 245 are located in the DNA-binding region of the protein, a section that generally encompasses residues 185–250. Why does the absence of GSTP cause such fundamental changes? Our results suggest a link between estrogen receptor–related effects and altered capabilities to maintain redox characteristics provided by GSTP. For example, we found that *S*-glutathionylation of ERα caused a mild reduction in receptor density (B_{max}) and reduced the affinity for 17β-estradiol. In contradistinction, palmitoylation of cysteine 447 (34, 35) of ERα enhances the binding affinity, indicating that the effects are dependent upon both the site and type of post-translational modification (36). Moreover, although there are somewhat limited results indicating that enhanced transcriptional activities correlate with increased binding affinity values, this relationship may not be universal (37), and other factors such as ERα dimer formation, translocation to cell compartments, altered half-life, or altered recognition of protein binding partners may play a role in regulating ERα functions. The fact that ERα has a comparatively large number of potential binding partners might also influence interpretation.

Dendritic cells are critical regulators of innate and acquired immunities, responding to stimuli, frequently downstream of toll-like receptors, that program them to undergo metabolic changes. Earlier results showed that toll-like receptor agonists caused BMDDCs to transition from oxidative phosphorylation to aerobic glycolysis, an event promoted by Akt signaling and inhibited by AMPK phosphorylation (38). Our present results suggest that ablation of GSTP is sufficient on its own to initiate similar kinase pathway responses and substantiate the involvement of mTOR signaling pathways as mediators of augmented energy production, particularly aerobic glycolysis, enhanced proliferation, and differentiation in BMDDCs. These pathway changes also establish a linear relationship with commensurate diminishment of *S*-glutathionylation of ERα.

Thus, the higher levels of *S*-glutathionylation of ERα in the wildtype BMDDCs alter its transcriptional activities and adjust gene expression patterns to favor proliferation and differentiation. In turn, this would provide an explanation of why *Gstp1/p2*$^{-/-}$ BMDDCs exhibit a glycolytic phenotype. Enhanced energy production can then give rise to an increased proinflammatory phenotype in these cells. Induction of glycolysis plays a central role for BMDDCs to acquire immunogenic properties following activation (21). Under non-inflammatory conditions, most BMDDCs exist in a quiescent, immature state and are poorly immunogenic. However, upon triggering of toll-like receptor by pathogen-derived products or inflammatory stimuli, BMDDCs undergo activation/maturation and are highly immunogenic. OXPHOS is associated with BMDDC quiescence, whereas BMDDC activation and immunogenicity rely heavily on glycolysis to provide carbon sources for *de novo* fatty acid synthesis to permit increased production and secretion of mediators. Comparing the quantitative RT-PCR data for the GSTP knockout and wildtype BMDDCs, a series of expression changes are consistent with the advancement of glycolysis. *Eno3* is an enolase glycolytic enzyme that catalyzes the reversible conversion of 2-phosphoglycerate to phosphoenolpyruvate. *Pgam1* is an isomerase that transfers a phosphate group from the C3 carbon of 3-phosphoglycerate to the C2 carbon, forming 2-phosphoglycerate. *Slc2a1* is the gene for GLUT1, a glucose transporter, highly conserved in humans and mice and is one of a family of 14 genes encoding GLUT proteins. It functions through maintenance of the low levels of basal glucose uptake required to sustain respiration. In cell membranes, GLUT1 levels can increase or decrease, respectively, in response to low or high glucose availability. It is important to remember that these alterations are found only as a consequence of ablation of GSTP. There is evidence that BMDDC functions may also be influenced by endoplasmic reticulum–induced stress, particularly as they relate as precursors of the unfolded protein response (39–42). We previously showed that markers for UPR, including IRE1 and ATF6, are constitutively higher in cells from *Gstp1/p2*$^{-/-}$ mice and that these animals have a narrower threshold of tolerance to oxidative stress compared with wildtype (24). In this regard, such data indicate that *Gstp1/p2*$^{-/-}$ mice are under higher levels of constitutive oxidative stress. Our present results indicate that LPS induces in BMDDCs the IRE1/XBP1 pathways linked with UPR and that the effects are more marked in *Gstp1/p2*$^{-/-}$ BMDDCs compared with wildtype (Fig. 4*E*).

Manipulation of metabolism of BMDDCs is quite critical as a determinant factor in mounting an immune response. The results that our *Gstp1/p2*$^{-/-}$ BMDDCs are more glycolytic and have a more proinflammatory phenotype suggest a potential for translational applications to assess whether pharmacological inhibition of GSTP can be used as a strategy to enhance the immunogenicity of BMDDCs in therapeutic settings. As such, the fact that redox intercepts estrogen-mediated signaling pathways provides a framework for linking those events that underlie immunity and bone marrow pathologies. For example, clinical results indicate that, in myeloma, patients homozygous for a variant allele of GSTP (one that we have shown to be less effective at catalyzing *S*-glutathionylation (43)) have greater progression-free survival (44). High levels of ERα are also present in the majority of multiple myeloma patient samples (45). Consequently, there may be a clinical correlate through lowered ERα *S*-glutathionylation levels in this patient population. Previously, the pharmaceutical inhibition of GSTP through the use of Telintra has proved effective in the management of myelodysplastic syndrome patients, in some cases causing the differentiation of precursor cancer cells, prior to establishment of a more malignant phenotype (15, 16). There are numerous other examples where drugs that alter redox homeostasis cause enhanced proliferation and functional changes in hematopoietic progenitor cells. At the simplest level, *N*-acetylcysteine (a precursor of cysteine) can enhance intracellular concentrations of GSH, reverse ROS suppression of N-cadherin–mediated hematopoietic stem cell adhesion to osteoblasts, and induce cell migration (46). Cysteine prodrugs can alter redox balance and enhance self-renewal of progenitor cells, whereas agents that diminish GSH, such as buthionine sulfoximine, can promote differentiation (4, 5). It appears that redox gradients in the marrow compartment are amenable to pharmacological manipulation, and altered redox gradients can influence HSC migration, differentiation, and myeloproliferation (9). Telintra continues to be developed in therapeutic settings, and its capacity to impair *S*-glutathionylation is a likely conduit to its clinical activities.

Experimental procedures

Mice

C57BL/6 wildtype mice were purchased from The Jackson Laboratory (Bar Harbor, ME). *Gstp1/p2*$^{-/-}$ mice were generated as described earlier (26). The mice were bred and kept in an Association for Assessment and Accreditation of Laboratory Animal Care – certified animal facility of the Medical University of South Carolina. All of the mice were used at ~8–12 weeks of age. The Institutional Animal Care and Use Committee of Medical University of South Carolina approved all the experimental procedures used in this study.

Primary BMDDC culture conditions

Immature bone marrow– derived dendritic cells were generated according to procedures reported previously (9). Briefly, BM cells ($4–5 \times 10^5$/ml, 10 ml/plate) were plated in RPMI 1640 medium (HyClone, Logan, UT) supplemented with 10% fetal bovine serum (FBS; Atlas Biologicals, Fort Collins, CO), 100 units/ml penicillin, 100 μg/ml streptomycin (all from Mediatech, Manassas, VA), and 20 ng/ml recombinant mouse GM-CSF (BioAbChem, Ladson, SC) (DC medium) into 100-mm culture dishes (Sarstedt, Newton, NC). Fresh DC medium was added on day 4 and gently replaced by fresh DC medium containing 10 ng/ml recombinant mouse GM-CSF on day 7. For mDCs, LPS (200 ng/ml; Sigma) was added to the culture described above, and the cells were cultured further overnight (~20 h).

Antibodies

The following antibodies were used for immunoblotting: rabbit monoclonal anti-ERα (Millipore, Burlington, MA;

04-820, Lot 2135146; 1:500 dilution); rabbit polyclonal anti-GSTP (MBL International, Woburn, MA; 311, Lot 071; 1:1000 dilution); mouse monoclonal anti-GSH (Virogen, Watertown, MA; 101-A, Lot GS-D8/G2-68; 1:1000 dilution); rabbit polyclonal anti-β-actin (ab8227, Lot GR60359-1), rabbit polyclonal anti-glucose transporter GLUT1 (ab32551, Lot GR208248-1), and goat polyclonal anti-GSTP (ab53943, Lot GR121458-9) (all from Abcam, Cambridge, MA; 1:1000 dilution); rabbit polyclonal anti-Akt (9272, Lot 24), rabbit polyclonal anti-phospho-Akt (Ser-473; 9271, Lot 22), mouse monoclonal anti-AMPK (2793, Lot 4), and rabbit polyclonal anti-phospho-AMPK (Thr-172; 2535, Lot 16) (all from Cell Signaling Technology, Danvers, MA; 1:500 dilution); mouse monoclonal anti-PGAM1 (sc-130334, Lot G0317) and mouse monoclonal anti-β-enolase (sc-10081, Lot G2417) (both from Santa Cruz Biotechnology, Dallas, TX; 1:200 dilution); and IRDye 800CW goat anti-mouse IgG (926-32210, Lot C20510-05), IRDye 800CW goat anti-rabbit IgG (926-32211, Lot C21227-02), 800CW donkey anti-goat IgG (926-32214, Lot C60119-05), IRDye 680RD goat anti-mouse IgG (926-68070, Lot C70427-05), IRDye 680RD goat anti-rabbit IgG (926-68071, Lot C20530-01), and IRDye 680RD donkey anti-goat IgG (926-68074, Lot C20606-04) (all from LI-COR Biosciences, Lincoln, NE; 1:15,000 dilution).

Immunoblotting

Total soluble protein was quantitated by BCA protein assay (Pierce). Cell lysates were resolved in SDS loading buffer (80 mM Tris-HCl, pH 6.8, 2% SDS, 10% glycerol, 0.02% bromphenol blue, $\pm$5 mM tris(2-carboxyethyl)phosphine) and heated at 95 °C for 5 min. Equal amounts of protein were electrophoretically separated by SDS-PAGE (Bio-Rad) and transferred onto Low Fluorescent PVDF membranes (Millipore) or nitrocellulose membranes (Bio-Rad) by a Trans-Blot Turbo Transfer System (Bio-Rad). PVDF or nitrocellulose membranes were incubated in Odyssey blocking buffer (LI-COR Biosciences) for 1 h to reduce nonspecific binding and then probed with appropriate primary antibodies (diluted in Odyssey blocking buffer) at 4 °C overnight. Immunoblots were then developed with infrared (IR) fluorescence IRDye secondary antibodies, imaged with a two-channel (red and green) IR fluorescence Odyssey CLx imaging system (LI-COR Biosciences), and quantified with Image Studio 4.0 software (LI-COR Biosciences).

Cell labeling and flow cytometry

Labeling was performed at room temperature using standard techniques. Cells were incubated with saturating concentrations of flow antibodies for 20 min, washed twice, and analyzed using a BD FACSVerse flow cytometer equipped with three lasers (407, 488, and 640 nm). 20,000 events per sample were acquired and analyzed using BD FACSuite software. The LIVE/DEAD Fixable Near-IR Dead Cell Stain kit (Invitrogen) was used to gate live cells. Data were analyzed with FlowJo software (Tree Star, Ashland, OR).

FITC-dextran uptake (endocytosis)

Immature dendritic cells were suspended in DC medium and incubated with 1 mg/ml FITC-dextran (molecular weight, 40,000; Sigma) for 4 h at 4 or 37 °C. The cells were washed two times with ice-cold PBS and 1% BSA and labeled with anti-mouse antibody mixture including APC-CD11c (from eBioscience, San Diego, CA) and PE-CD3e, PE-CD45R/B220, PE-CD14, and PE-NK1.1 (all from BD Pharmingen). The cells were washed two times, fixed with 2% paraformaldehyde, and analyzed by flow cytometry. The uptake was calculated as the change in MFI between cell samples incubated at 37 and 4 °C.

ELISAs

Measurements of IL-12p70 and IL-10 in imDC or mDC supernatants were performed using the ELISA Ready-Set-Go! Reagent set from eBioscience according to the manufacturer's protocol.

DC–T cell coculture

Splenocytes from *Pmel-1* TCR transgenic C57BL/6 mice were depleted of erythrocytes by ammonium-chloride-potassium lysing buffer (Life Technologies). Isolation of T cells was achieved using the Dynabeads Untouched Mouse T Cells kit (Life Technologies) according to the manufacturer's protocol. Isolated T cells were labeled with 2.5 μM intracellular fluorescent dye CFSE (Life Technologies) and then cocultured (1×10^6 cells/well) with hgp100(25–33)-pulsed (1 μg/ml for 2 h) mDCs (2×10^5 cells/well) in 48-well plates (Sarstedt) in T-cell medium (RPMI 1640 medium supplemented with 10% FBS, 100 units/ml penicillin, 100 μg/ml streptomycin, 1 mM sodium pyruvate, 1$\times$ nonessential amino acids, 10 ng/ml recombinant mouse IL-2 (BioAbChem)). After 3 days, the cells were labeled with anti-mouse PE-CD8a (BD Pharmingen), and T-cell proliferation was analyzed by flow cytometry. As a control, splenocytes from *Pmel-1* TCR transgenic mouse were labeled with CFSE, cultured in T-cell medium in the presence of 1 μg/ml hgp100(25–33) for 3 days, and examined for T-cell proliferation.

Measurement of intracellular ROS

Intracellular ROS was measured using the OxiSelect *In Vitro* ROS/RNS kit from Cell Biolabs (San Diego, CA) according to the manufacturer's protocol. Briefly, BMDDCs ($1.0–2.0 \times 10^6$ cells/ml) were suspended in DC medium and incubated with 200 ng/ml LPS at 37 °C at the indicated times. Cells were harvested and solubilized by ice-cold lysis buffer (50 mM Tris-HCl pH 7.5, 150 mM NaCl, 1% Triton, 1 mM EDTA, 1 mM EGTA, protease inhibitor mixture (Roche Applied Science/Sigma)). Cell lysates were collected and immediately subjected to the ROS/RNS measurement. The fluorescence intensity of fluorophore dichlorofluorescein, which was formed by peroxide oxidation of the non-fluorescent precursor dichlorodihydrofluorescin (DCFH), was detected at 480-nm excitation/530-nm emission using a SpectraMax M5 Multi-Mode microplate reader (Molecular Devices, Sunnyvale, CA). DCFH with lysis buffer was used as a blank control.

Measurement of intracellular reduced thiol levels

Immature DCs ($1.0–2.0 \times 10^6$cells/ml) were suspended in DC medium and incubated with 200 ng/ml LPS overnight at 37 °C. Cells were harvested and solubilized by ice-cold lysis buffer as mentioned above. Cell lysates were collected and

immediately subjected to reduced thiol measurement using thiol fluorescent probe IV (Millipore). Fluorescence intensities were detected at 400-nm excitation/465-nm emission using a microplate reader. Thiol fluorescent probe IV with lysis buffer was used as a blank control.

Measurement of surface reduced thiol levels

ThioGlo-1 (TG-1; Calbiochem) was used to monitor the cell surface reduced thiols as reported earlier (11). Briefly, BMDDCs (1.0×10^6 cells/ml) were suspended in PBS and 100 μM $CaCl_2$ and stimulated with 200 ng/ml LPS for the indicated times. Total surface reduced thiol levels were then determined by an immediate fluorescence increase upon addition of TG-1 (final concentration, 5 μM) at 379-nm excitation/513-nm emission, measured by a QuantaMaster spectrofluorometer equipped with an A-1010B continuous xenon arc lamp and an 814 Photomultiplier Detection System (Photon Technology International, Birmingham, NJ) in a quartz cuvette under constant stirring at 37 °C, controlled by a TC 125 temperature controller (Quantum Northwest, Shoreline, WA). The emission of each sample was recorded for 30 s (background) before and until 250 s after the addition of TG-1 (resolution, 0.1 s). Saturated TG-1 fluorescence values were corrected for background emissions, normalized for cell numbers, and averaged using SigmaPlot 10.0 software (Systat Software, San Jose, CA).

Measurement of GSH and GSSG levels

Quantitative determinations of GSH and GSSG levels were performed using the enzymatic recycling method (48). Briefly, protein in the cell extracts was precipitated by sulfosalicylic acid, and the supernatant was then divided into two parts. For reduced GSH, the supernatant was incubated with thiol fluorescent probe IV, and fluorescence intensities were measured at 400-nm excitation/465-nm emission. For total GSH (GSH + GSSG), the supernatant was neutralized by triethanolamine and incubated with the reduction system (containing NADPH and glutathione reductase) at 37 °C for 20 min. GSSG was calculated based on the results from reduced GSH and total GSH; the ratio of GSH/GSSG = [GSH]/(([Total GSH] − [GSH])/2).

Glucose uptake

Glucose uptake was determined by 2-NBDG (Cayman Chemical, Ann Arbor, MI) according to the manufacture's protocol. 2-NBDG is a fluorescently labeled deoxyglucose analog. Briefly, imDCs or mDCs (0.2×10^6 cells/well in 100 μl) were seeded in a 96-well black clear-bottom plate (Greiner) in glucose- and pyruvate-free RPMI 1640 medium and incubated with 100 μg/ml 2-NBDG at 37 °C at the indicated times. Cells were washed with PBS and resuspended in 200 μl of PBS, and the fluorescence intensities were measured at 485-nm excitation/535-nm emission using a microplate reader.

Proteomic analyses: Identification of S-glutathionylated cysteine

Recombinant human ERα protein (Thermo Fisher Scientific, Waltham, MA) (UniProtKB P03372) was *S*-glutathionylated and separated on a non-reducing gel. Following colloidal Coomassie staining with ProtoBlue Safe (National Diagnostics, Atlanta, GA), bands were excised, destained, and enzymatically digested with porcine trypsin (Sigma) at a 1:20 enzyme/protein ratio sequentially with lysyl endopeptidase (Wako, Richmond, VA) and Asp-N (Roche Applied Science/Sigma) at a 1:20 enzyme/protein ratio or with Glu-C (Thermo Fisher Scientific) at a 1:15 enzyme/protein ratio. Digestions were performed at 37 °C for 15 h with agitation in 100 mM ammonium bicarbonate. The digested peptides were extracted with 5% formic acid in 50% acetonitrile or 85% acetonitrile sequentially and dried under vacuum, and particulates were removed using a μC_{18} ZipTip (Millipore).

LC-MS/MS

Peptides dissolved in 2% formic acid, 2% acetonitrile were loaded onto a C_{18} PepMap 100 (300-μm × 5-mm) trap column (Thermo Fisher Scientific) for 10 min at 30 μl/min and separated on a 75-μm internal diameter × 15-cm fused-silica column packed in house with ReproSil-Pur 120 C_{18}-AQ (1.9 μm; Dr. Maisch GmbH, Germany) at 180 nl/min using a gradient of 5–50% solvent B in 180 min on an LC Packings U3000 Nano LC system. Solvent A was 0.2% formic acid in 5% acetonitrile; solvent B was 0.2% formic acid in 80% acetonitrile. Peptides were mass-analyzed on a Thermo Orbitrap Elite with alternating collision-induced dissociation (CID) and electron transfer dissociation (ETD) fragmentation. Mass spectra were acquired in data-dependent mode using a top 7 method. Each FTMS survey scan was acquired with a mass range of m/z 400–1700 in the Orbitrap followed by acquisition of the tandem mass spectra of the seven most intense ions in the dual-pressure ion trap. The automatic gain control (AGC) target value in the Orbitrap was 10^6 for the survey FTMS scan at a resolution of 60,000 at m/z 400. A normalized collision energy of 35% was used for CID with an AGC of 1000. The ETD reaction time was adjusted based on the charge state of the ion, AGC was set to 10^4 ions, and supplemental activation was enabled. The threshold for triggering CID and ETD was 500. Dynamic exclusion was enabled with a repeat count of 1 (or 2 depending on the run), repeat duration of 30 s, and exclusion duration of 180 s. The chromatography feature was enabled for all runs. Lock mass was not utilized. Targeted LC-MS/MS analyses were also performed using inclusion masses for predicted *S*-glutathionylated peptides.

Database searching

The CID and ETD MS/MS spectra were searched using Mascot (version 2.4.01) and SEQUEST HT search algorithms within Proteome Discoverer 1.4 (Thermo Fisher Scientific) against a UniProtKB human database (Swiss-Prot + TrEMBL downloaded on August 23, 2016) containing 154,527 entries plus digestion enzymes. For both algorithms, the search parameters allowed for three missed cleavages, precursor mass tolerances of ±25 ppm, and fragment mass tolerances ±0.8 Da. Dynamic modifications on cysteines included glutathionylation (+305.0682 Da with a +129.0426-Da neutral loss), conversion of cysteine to dehydroalanine (−33.9877 Da), sulfide (+31.9721 Da), and trioxidation (+47.9847 Da). Methionine oxidation was also used as a variable modification. Tandem mass spectra were also searched using the Andromeda algorithm within MaxQuant version 1.5.5.1 (23) using the same

database and modifications as above. Following recalibration, peptides were filtered using a 4.5-ppm precursor mass tolerance. CID and ETD spectra were also converted to "Mascot generic format (mgf)" and searched using Protein Prospector version 5.19.1 (47) against the estrogen receptor sequence (P03372) with the same variable modifications as above, including searching for disulfide linkages.

All identified spectra were manually inspected. The ETD spectra of *S*-glutathionylated peptides with charge states greater than +2 were inspected for the presence of the diagnostic glutathione ion at *m*/*z* 308. Both the CID and ETD spectra were also inspected for the presence of fragments originated by the loss of glutathione (−305 Da) or the neutral loss of glutamic acid (−129 Da). The characteristic fragmentation pattern and expected neutral losses of *S*-glutathionylated peptides are shown in the supporting information.

Estrogen receptor binding assays

Saturation binding assays of estradiol with ERα were performed using [^{3}H]estradiol (Moraver, Brea, CA). Briefly, recombinant human ERα protein (untreated or treated with disulfiram to induce *S*-glutathionylation) was incubated with [^{3}H]estradiol (from 0.625 to 80 nM) in assay buffer (100 mM Tris-HCl, 1 mM EDTA, 1 mM EGTA, protease inhibitor mixtures, 10% glycerol, 10 mg/ml BSA, pH 7.4) at room temperature for 90 min; unbound [^{3}H]estradiol was then removed by adding the same amount of 0.4% dextran-coated charcoal (Activated Charcoal Norit®, Sigma) suspension (freshly prepared). After incubating for 10 min on ice, suspensions were centrifuged at 13,000 rpm for 10 min, and supernatants were subjected to liquid scintillation counting. Data were analyzed using a specific binding module from Prism 5.0. Maximum amounts of estradiol bound receptor (B_{max}) and binding affinities (K_d) were calculated.

OCR and ECAR analyses

OCR and ECAR analyses were performed using an XF-96 Extracellular Flux Analyzer (Seahorse Bioscience). Briefly, BMDDCs (70,000 cells/well in 70 μl) were seeded in an XF-96 cell culture plate and either left unstimulated or stimulated with 200 ng/ml LPS overnight. Cells were washed and analyzed in XF running buffer according to the manufacturer's instructions to obtain real-time measurement of OCR and ECAR. Where indicated, OCR and ECAR were analyzed in response to 1 μM oligomycin, 1.5 μM carbonyl cyanide *p*-trifluoromethoxyphenylhydrazone, and 100 nM rotenone plus 1 μM antimycin (all from Sigma).

RNA isolation and RT-PCR

Total RNA was prepared using the Isolate II RNA Mini kit (Bioline, Taunton, MA), and cDNA was then generated with the iScript cDNA synthesis kit (Bio-Rad) according to the manufacturers' protocols. Subsequently, quantification of gene expression was performed in duplicates using iQ™ SYBR® Green Supermix (Bio-Rad) with detection on a MyiQ™ Real-Time PCR System (Bio-Rad). The reaction cycles used were 95 °C for 5 min and then 40 cycles at 95 °C for 15 s and 58 °C for 1 min followed by melt curve analysis. The following primers were used: *Aldoa*: forward 5′-TCAGTGCTGGGTATGGGTG-3′, reverse 5′-GCTCCTTAGTCCTTTCGCCT-3′; *Aldoc*: forward, 5′-GCGGGCAGAGATGAACGGGC-3′; reverse, 5′-AGAGGGACTGTGCTGCCGCT-3′; *Eno1*: forward, 5′-AAAGATCTCTCTGGCGTGGAC-3′; reverse, 5′-CTTAACGCTCTCCTCGGTGT-3′; *Eno3*: forward, 5′-GGACTCCAGGGGCAACCCCA-3′; reverse, 5′-TGCTCGGAATCGACCCTTGGC-3′; *Esr1*: forward, 5′-CCTCCCGCCTTCTACAGGT-3′; reverse, 5′-CACACGGCACAGTAGCGAG-3′; *Gapdh*: forward, 5′-CCCAGCAAGGACACTGAGCAA-3′; reverse, 5′-AGGCCCCTCCTGTTATTATGG-3′; *Gck*: forward, 5′-GCTCAGTGAACCCCGGTCAGC-3′; reverse, 5′-TGTGCGCAGCTGCTCTGAGG-3′; *Gpi*: forward, 5′-GCTGGCCAAGTCCAGAGGCG-3′; reverse, 5′-ACCGCCCGATCCTCGGTGTA-3′; *Hk2*: forward, 5′-GGAACCGCCTAGAAATCTCC-3′; reverse, 5′-GGAGCTCAACCAAAACCAAG-3′; *Ldha*: forward, 5′-TGTCTCCAGCAAAGACTACTGT-3′; reverse, 5′-GACTGTACTTGACAATGTTGGGA-3′; *Ldhb*: forward, 5′-CCCAGCAGCTGCCACGGATG-3′; reverse, 5′-CCGCTCCACACAGCCACACT-3′; *Ldhc*: forward, 5′-TGCGGAGTCAGCAGTAAGGCTC-3′; reverse, 5′-AGCACACGCCATGCCCACAT-3′; *Nd4*: forward, 5′-ATTATTATTACCCGATGAGGGAACC-3′; reverse, 5′-ATTAAGATGAGGGCAATTAGCAGT-3′; *Pfk*: forward, 5′-AGGAGGGCAAAGGAGTGTTT-3′; reverse, 5′-TTGGCAGAAATCTTGGTTCC-3′; *Pgam1*: forward, 5′-TCTGCACAGAGGTGAAGCAG-3′; reverse, 5′-GTACGACGCCGACCTGAG-3′; *Pgk1*: forward, 5′-GGAGGCCCGGCATTCTGCAC-3′; reverse, 5′-AGTCCACCCTCATCACGACCCG-3′; *pkm*: forward, 5′-GTCTGAATGAAGGCAGTCCC-3′; reverse, 5′-GTCCGCTCTAGGTATCGCAG-3′; *Slc2a1*: forward, 5′-GGCCGCCTCATGTTGGCTGT-3′, reverse, 5′-TGGGCTCTCCGTAGCGGTGG-3′; *Slc2a4*: forward, 5′-GTGACTGGAACACTGGTCCTA-3′; reverse, 5′-CCAGCCACGTTGCATTGTAG-3′. A mouse estrogen receptor signaling PrimePCR™ pathway array plate was purchased from Bio-Rad, the genes were listed in supporting Table S1, and expression of genes was evaluated by determining mRNA levels in day 7 BMDDCs. Relative gene expression quantification was based on the comparative threshold cycle (CT) method ($2^{-\Delta\Delta CT}$) with normalization of the raw data to the included housekeeping gene (*Gapdh*). PrimePCR gene expression was analyzed using Bio-Rad PrimePCR Analysis software.

Statistical analysis

Student's *t* tests were used to analyze significant differences. *p* values <0.05 were regarded as statistically significant. Data were expressed as means ± S.D.

Author contributions—D. M. T., K. D. T., J. Z., Z.-w. Y., and S. M. designed the study. J. Z., Z.-w. Y., W. C., and Y. M. performed experiments and assisted D. M. T., K. D. T., and Y. J.-H. in analyzing data. L. B. performed proteomic analyses. D. M. T., K. D. T., J. Z., Z.-w. Y., and Y. J.-H. wrote the manuscript.

Acknowledgment—This work was conducted in a facility constructed with support from National Institutes of Health Grant C06 RR015455 from the Extramural Research Facilities Program of the National Center for Research Resources.

References

1. Ballesteros-Tato, A., León, B., Lund, F. E., and Randall, T. D. (2010) Temporal changes in dendritic cell subsets, cross-priming and costimulation via CD70 control $CD8^+$ T cell responses to influenza. *Nat. Immunol.* **11,** 216–224 CrossRef Medline
2. Nakano, H., Lin, K. L., Yanagita, M., Charbonneau, C., Cook, D. N., Kakiuchi, T., and Gunn, M. D. (2009) Blood-derived inflammatory dendritic cells in lymph nodes stimulate acute T helper type 1 immune responses. *Nat. Immunol.* **10,** 394–402 CrossRef Medline
3. Hashimoto, D., Miller, J., and Merad, M. (2011) Dendritic cell and macrophage heterogeneity *in vivo*. *Immunity* **35,** 323–335 CrossRef Medline
4. Murata, Y., Shimamura, T., and Hamuro, J. (2002) The polarization of T_h1/T_h2 balance is dependent on the intracellular thiol redox status of macrophages due to the distinctive cytokine production. *Int. Immunol* **14,** 201–212 CrossRef Medline
5. Hadzic, T., Li, L., Cheng, N., Walsh, S. A., Spitz, D. R., and Knudson, C. M. (2005) The role of low molecular weight thiols in T lymphocyte proliferation and IL-2 secretion. *J. Immunol.* **175,** 7965–7972 CrossRef Medline
6. Arai, F., Yoshihara, H., Hosokawa, K., Nakamura, Y., Gomei, Y., Iwasaki, H., and Suda, T. (2009) Niche regulation of hematopoietic stem cells in the endosteum. *Ann. N.Y. Acad. Sci.* **1176,** 36–46 CrossRef Medline
7. Calvi, L. M., Adams, G. B., Weibrecht, K. W., Weber, J. M., Olson, D. P., Knight, M. C., Martin, R. P., Schipani, E., Divieti, P., Bringhurst, F. R., Milner, L. A., Kronenberg, H. M., and Scadden, D. T. (2003) Osteoblastic cells regulate the haematopoietic stem cell niche. *Nature* **425,** 841–846 CrossRef Medline
8. Grek, C. L., Townsend, D. M., and Tew, K. D. (2011) The impact of redox and thiol status on the bone marrow: pharmacological intervention strategies. *Pharmacol. Ther.* **129,** 172–184 CrossRef Medline
9. Zhang, J., Ye, Z. W., Gao, P., Reyes, L., Jones, E. E., Branham-O'Connor, M., Blumer, J. B., Drake, R. R., Manevich, Y., Townsend, D. M., and Tew, K. D. (2014) Glutathione S-transferase P influences redox and migration pathways in bone marrow. *PLoS One* **9,** e107478, CrossRef Medline
10. Eylar, E., Rivera-Quinones, C., Molina, C., Báez, I., Molina, F., and Mercado, C. M. (1993) N-Acetylcysteine enhances T cell functions and T cell growth in culture. *Int. Immunol* **5,** 97–101 CrossRef Medline
11. Townsend, D. M., He, L., Hutchens, S., Garrett, T. E., Pazoles, C. J., and Tew, K. D. (2008) NOV-002, a glutathione disulfide mimetic, as a modulator of cellular redox balance. *Cancer Res.* **68,** 2870–2877 CrossRef Medline
12. List, A. F., Brasfield, F., Heaton, R., Glinsmann-Gibson, B., Crook, L., Taetle, R., and Capizzi, R. (1997) Stimulation of hematopoiesis by amifostine in patients with myelodysplastic syndrome. *Blood* **90,** 3364–3369 Medline
13. Townsend, D. M., Manevich, Y., He, L., Hutchens, S., Pazoles, C. J., and Tew, K. D. (2009) Novel role for glutathione *S*-transferase Pi. Regulator of protein *S*-glutathionylation following oxidative and nitrosative stress. *J. Biol. Chem.* **284,** 436–445 CrossRef Medline
14. Ruscoe, J. E., Rosario, L. A., Wang, T., Gaté, L., Arifoglu, P., Wolf, C. R., Henderson, C. J., Ronai, Z., and Tew, K. D. (2001) Pharmacologic or genetic manipulation of glutathione S-transferase P1-1 (GSTpi) influences cell proliferation pathways. *J. Pharmacol. Exp. Ther.* **298,** 339–345 Medline
15. Raza, A., Galili, N., Callander, N., Ochoa, L., Piro, L., Emanuel, P., Williams, S., Burris, H., 3rd, Faderl, S., Estrov, Z., Curtin, P., Larson, R. A., Keck, J. G., Jones, M., Meng, L., *et al.* (2009) Phase 1–2a multicenter dose-escalation study of ezatiostat hydrochloride liposomes for injection (Telintra, TLK199), a novel glutathione analog prodrug in patients with myelodysplastic syndrome. *J. Hematol. Oncol.* **2,** 20 CrossRef Medline
16. Lyons, R. M., Wilks, S. T., Young, S., and Brown, G. L. (2011) Oral ezatiostat HCl (Telintra(R), TLK199) and idiopathic chronic neutropenia (ICN): a case report of complete response of a patient with G-CSF resistant ICN following treatment with ezatiostat, a glutathione S-transferase P1-1 (GSTP1-1) inhibitor. *J. Hematol. Oncol.* **4,** 43 CrossRef Medline
17. Gate, L., Majumdar, R. S., Lunk, A., and Tew, K. D. (2004) Increased myeloproliferation in glutathione *S*-transferase Pi-deficient mice is associated with a deregulation of JNK and Janus kinase/STAT pathways. *J. Biol. Chem.* **279,** 8608–8616 CrossRef Medline
18. Kovats, S. (2012) Estrogen receptors regulate an inflammatory pathway of dendritic cell differentiation: mechanisms and implications for immunity. *Horm. Behav.* **62,** 254–262 CrossRef Medline
19. Michalek, R. D., Gerriets, V. A., Nichols, A. G., Inoue, M., Kazmin, D., Chang, C. Y., Dwyer, M. A., Nelson, E. R., Pollizzi, K. N., Ilkayeva, O., Giguere, V., Zuercher, W. J., Powell, J. D., Shinohara, M. L., McDonnell, D. P., *et al.* (2011) Estrogen-related receptor-alpha is a metabolic regulator of effector T-cell activation and differentiation. *Proc. Natl. Acad. Sci. U.S.A.* **108,** 18348–18353 CrossRef Medline
20. Everts, B., Amiel, E., van der Windt, G. J., Freitas, T. C., Chott, R., Yarasheski, K. E., Pearce, E. L., and Pearce, E. J. (2012) Commitment to glycolysis sustains survival of NO-producing inflammatory dendritic cells. *Blood* **120,** 1422–1431 CrossRef Medline
21. Everts, B., and Pearce, E. J. (2014) Metabolic control of dendritic cell activation and function: recent advances and clinical implications. *Front. Immunol.* **5,** 203 CrossRef Medline
22. Pearce, E. J., and Everts, B. (2015) Dendritic cell metabolism. *Nat. Rev. Immunol* **15,** 18–29 CrossRef Medline
23. Cox, J., and Mann, M. (2008) MaxQuant enables high peptide identification rates, individualized p.p.b.-range mass accuracies and proteome-wide protein quantification. *Nat. Biotechnol.* **26,** 1367–1372 CrossRef Medline
24. Ye, Z. W., Zhang, J., Ancrum, T., Manevich, Y., Townsend, D. M., and Tew, K. D. (2017) Glutathione S-transferase P-mediated protein S-glutathionylation of resident endoplasmic reticulum proteins influences sensitivity to drug-induced unfolded protein response. *Antioxid. Redox Signal.* **26,** 247–261 CrossRef Medline
25. Sonoda, J., Laganière, J., Mehl, I. R., Barish, G. D., Chong, L. W., Li, X., Scheffler, I. E., Mock, D. C., Bataille, A. R., Robert, F., Lee, C. H., Giguère, V., and Evans, R. M. (2007) Nuclear receptor ERRα and coactivator PGC-1β are effectors of IFN-γ-induced host defense. *Genes Dev.* **21,** 1909–1920 CrossRef Medline
26. Henderson, C. J., Smith, A. G., Ure, J., Brown, K., Bacon, E. J., and Wolf, C. R. (1998) Increased skin tumorigenesis in mice lacking pi class glutathione S-transferases. *Proc. Natl. Acad. Sci. U.S.A.* **95,** 5275–5280 CrossRef Medline
27. Giguère, V. (2008) Transcriptional control of energy homeostasis by the estrogen-related receptors. *Endocr. Rev.* **29,** 677–696 CrossRef Medline
28. Igarashi, H., Kouro, T., Yokota, T., Comp, P. C., and Kincade, P. W. (2001) Age and stage dependency of estrogen receptor expression by lymphocyte precursors. *Proc. Natl. Acad. Sci. U.S.A.* **98,** 15131–15136 CrossRef Medline
29. Carreras, E., Turner, S., Paharkova-Vatchkova, V., Mao, A., Dascher, C., and Kovats, S. (2008) Estradiol acts directly on bone marrow myeloid progenitors to differentially regulate GM-CSF or Flt3 ligand-mediated dendritic cell differentiation. *J. Immunol.* **180,** 727–738 CrossRef Medline
30. Hayes, J. D., Flanagan, J. U., and Jowsey, I. R. (2005) Glutathione transferases. *Annu. Rev. Pharmacol. Toxicol.* **45,** 51–88 CrossRef Medline
31. Townsend, D. M., Lushchak, V. I., and Cooper, A. J. (2014) A comparison of reversible versus irreversible protein glutathionylation. *Adv. Cancer Res.* **122,** 177–198 CrossRef Medline
32. Townsend, D. M., Manevich, Y., He, L., Xiong, Y., Bowers, R. R., Jr, Hutchens, S., and Tew, K. D. (2009) Nitrosative stress-induced S-glutathionylation of protein disulfide isomerase leads to activation of the unfolded protein response. *Cancer Res.* **69,** 7626–7634 CrossRef Medline
33. Aliau, S., El Garrouj, D., Yasri, A., Katzenellenbogen, B. S., and Borgna, J. L. (1997) 17α-(Haloacetamidoalkyl) estradiols alkylate the human estrogen receptor at cysteine residues 417 and 530. *Biochemistry* **36,** 5861–5867 CrossRef Medline
34. Acconcia, F., Ascenzi, P., Bocedi, A., Spisni, E., Tomasi, V., Trentalance, A., Visca, P., and Marino, M. (2005) Palmitoylation-dependent estrogen receptor alpha membrane localization: regulation by 17β-estradiol. *Mol. Biol. Cell* **16,** 231–237 CrossRef Medline
35. Marino, M., Ascenzi, P., and Acconcia, F. (2006) S-Palmitoylation modulates estrogen receptor alpha localization and functions. *Steroids* **71,** 298–303 CrossRef Medline

36. Lin, A. H., Li, R. W., Ho, E. Y., Leung, G. P., Leung, S. W., Vanhoutte, P. M., and Man, R. Y. (2013) Differential ligand binding affinities of human estrogen receptor-α isoforms. *PLoS One* **8,** e63199 CrossRef Medline
37. Klinge, C. M. (2001) Estrogen receptor interaction with estrogen response elements. *Nucleic Acids Res.* **29,** 2905–2919 CrossRef Medline
38. Krawczyk, C. M., Holowka, T., Sun, J., Blagih, J., Amiel, E., DeBerardinis, R. J., Cross, J. R., Jung, E., Thompson, C. B., Jones, R. G., and Pearce, E. J. (2010) Toll-like receptor-induced changes in glycolytic metabolism regulate dendritic cell activation. *Blood* **115,** 4742–4749 CrossRef Medline
39. Martinon, F., Chen, X., Lee, A. H., and Glimcher, L. H. (2010) TLR activation of the transcription factor XBP1 regulates innate immune responses in macrophages. *Nat. Immunol.* **11,** 411–418 CrossRef Medline
40. Goodall, J. C., Wu, C., Zhang, Y., McNeill, L., Ellis, L., Saudek, V., and Gaston, J. S. (2010) Endoplasmic reticulum stress-induced transcription factor, CHOP, is crucial for dendritic cell IL-23 expression. *Proc. Natl. Acad. Sci. U.S.A.* **107,** 17698–17703 CrossRef Medline
41. Osorio, F., Tavernier, S. J., Hoffmann, E., Saeys, Y., Martens, L., Vetters, J., Delrue, I., De Rycke, R., Parthoens, E., Pouliot, P., Iwawaki, T., Janssens, S., and Lambrecht, B. N. (2014) The unfolded-protein-response sensor IRE-1α regulates the function of CD8α+ dendritic cells. *Nat. Immunol.* **15,** 248–257 CrossRef Medline
42. Iwakoshi, N. N., Pypaert, M., and Glimcher, L. H. (2007) The transcription factor XBP-1 is essential for the development and survival of dendritic cells. *J. Exp. Med.* **204,** 2267–2275 CrossRef Medline
43. Manevich, Y., Hutchens, S., Tew, K. D., and Townsend, D. M. (2013) Allelic variants of glutathione S-transferase P1-1 differentially mediate the peroxidase function of peroxiredoxin VI and alter membrane lipid peroxidation. *Free Radic. Biol. Med.* **54,** 62–70 CrossRef Medline
44. Dasgupta, R. K., Adamson, P. J., Davies, F. E., Rollinson, S., Roddam, P. L., Ashcroft, A. J., Dring, A. M., Fenton, J. A., Child, J. A., Allan, J. M., and Morgan, G. J. (2003) Polymorphic variation in GSTP1 modulates outcome following therapy for multiple myeloma. *Blood* **102,** 2345–2350 CrossRef Medline
45. Otsuki, T., Yamada, O., Kurebayashi, J., Moriya, T., Sakaguchi, H., Kunisue, H., Yata, K., Uno, M., Yawata, Y., and Ueki, A. (2000) Estrogen receptors in human myeloma cells. *Cancer Res.* **60,** 1434–1441 Medline
46. Jang, Y. Y., and Sharkis, S. J. (2007) A low level of reactive oxygen species selects for primitive hematopoietic stem cells that may reside in the low-oxygenic niche. *Blood* **110,** 3056–3063 CrossRef Medline
47. Trnka, M. J., Baker, P. R., Robinson, P. J., Burlingame, A. L., and Chalkley, R. J. (2014) Matching cross-linked peptide spectra: only as good as the worse identification. *Mol. Cell. Proteomics* **13,** 420–434 CrossRef Medline
48. Rahman, I., Kode, A., and Biswas, S. K. (2006) Assay for quantitative determination of glutathione and glutathione disulfide levels using enzymatic recycling method. *Nat. Protoc.* **1,** 3159–3165 CrossRef Medline